ADVANCED FUNCTIONAL MATERIALS

BIOMEDICAL SENSORS

J. A. Rogers and co-workers present an ultrathin, skin-like device for the wireless measurement of the dielectric properties and deformations of the skin. The construction exploits LC resonators with capacitive electrodes that are responsive to skin properties. The material designs offer the potential for compact, epidermal, wireless systems in applications ranging from dermatology and cosmetology to health/wellness monitoring. The image shows the application of lotion onto a skin region that supports a representative device.

WILEY-VCH

FULL PAPER

Materials and Designs for Wireless Epidermal Sensors of Hydration and Strain

*Xian Huang, Yuhao Liu, Huanyu Cheng, Woo-Jung Shin, Jonathan A. Fan, Zhuangjian Liu, Ching-Jui Lu, Gil-Woo Kong, Kaile Chen, Dwipayan Patnaik, Sang-Heon Lee, Sami Hage-Ali, Yonggang Huang, and John A. Rogers**

This paper presents materials and designs for an ultrathin, stretchable class of device that is capable of lamination onto the surface of the skin, for wireless determination of dielectric and surface strain properties. The sensor exploits LC resonators with capacitive electrodes whose radio frequency characteristics change with variations in skin properties, and is capable of conformal and spontaneous integration with skin due to their skin-like, "epidermal", mechanical properties. Resonance frequencies of the LC resonators can be measured wirelessly through changes in the absorption of electromagnetic energy from a coil connected to an impedance measurement setup and placed in proximity to the epidermal device. Experimental results demonstrate that the device offers a precision of 1.1 (arbitrary unit of a reference commercial hydration meter) for hydration and 1.3% for strain detection, with good stability and low drift. Measurement of simulated lymphedema using an expandable balloon with an attached sensor further demonstrates the potential for using such a sensor in monitoring skin swelling. Finite element simulation of physical deformation and associated changes in electrical properties enable quantitative interpretation of the experimental results. The results may have relevance for wireless evaluation of the skin, for applications ranging from dermatology and cosmetology to health/wellness monitoring (lymphedema, transdermal water loss, edema, and psychological stress).

1. Introduction

Biomedical sensors that use rigid, planar metal electrodes on hard substrates have mechanical properties that are significantly different from those of the soft, curved, and textured surfaces of biological tissues. This mismatch results in diminished measurement accuracy and precision, due to variability at the point of electrode/tissue contact. Dry electrodes based on ultrathin flexible polymer films (e.g., parylene)[1,2] and elastomer substrates (e.g., polydimethylsiloxane, PDMS)[3,4] offer improved capabilities, due partly to their enhanced levels of conformability, defined as the capability of the device to establish intimate contact with the soft, textured surface of the skin. In many cases, additional fixtures are required to achieve robust adhesion to the skin.[5,6] Sensors with "epidermal" construction, in which the mechanical properties, thermal loads (≈150 μJ cm^{-2} K^{-1}),[7] area mass densities (<3.8 mg cm^{-2})[8] and thicknesses (<10 μm) are in the range of the epidermis, can provide intimate skin contact based on Van der Waals forces, likely due to London-dispersion effects between molecules of the skin and the elastomer substrate (e.g., PDMS), thereby eliminating the need of pins, straps, tapes or adhesives.[9] This type of contact offers opportunities in highly repeatable and precise determination not only of properties of the skin itself, but of overall health status in which the skin provides an interface for measurement of internal body processes. Several types of epidermal sensors have been previously reported, for determination of skin impedance,[10] electrophysiological potentials,[11] temperature,[7] and mechanical strain.[12] The major drawback of previously published work in the field of epidermal sensors is that most rely on wired connections to signal acquisition equipment, limiting their use in long-term, continuous monitoring.

One appealing approach to epidermal wireless sensing relies on passive inductive coupling, in which changes in the sensing components alter the frequencies of resonant circuits made of inductors and capacitors. This method, usually

Dr. X. Huang, Y. Liu, W.-J. Shin, Dr. J. A. Fan, C.-J. Lu, G.-W. Kong, K. Chen, D. Patnaik, S.-H. Lee, Dr. S. Hage-Ali, Prof. J. A. Rogers
University of Illinois at Urbana-Champaign
Frederick Seitz Materials Research Laboratory
104 S. Goodwin Ave, Urbana, IL 61801, USA
E-mail: jrogers@illinois.edu
H. Cheng, Prof. Y. Huang
Northwestern University
Mechanical Engineering
2145 Sheridan Road, TECH #A116 Evanston
IL 60208, USA
Dr. Z. Liu
Institute of High Performance Computing
1 Fusionopolis Way, #16–16 Connexis
Singapore 138632, Singapore

DOI: 10.1002/adfm.201303886

referred to as wireless passive sensing,[13] provides a convenient scheme that does not require active components or power supplies, thereby making it well suited for epidermal integration. Previously reported passive wireless sensors, in conventional, non-epidermal formats, offer capabilities for measurement of intraocular pressure,[14,15] gas flow,[16] cerebrospinal fluid shunt function,[17] blood pressure,[18] and cardiovascular pressure.[19]

Realizing these types of systems in epidermal constructs, and optimizing their use in sensors that have simultaneous capabilities of measuring the dielectric and mechanical strain properties of the skin represents the topic of the present report. Skin dielectric measurements serve as effective monitors of various physiological processes,[20–22] and can be conducted at different frequencies for information related to different skin depths[23,24] and conditions.[24] At frequencies of hundreds of MHz, the effects of relaxation of water molecules dominate. Here, skin dielectric measurements can reveal dermatological and cosmetological effects related to water content in the skin, including wound healing,[25] thermal injury,[26] therapeutic activity,[27,28] and abnormal skin conditions, including edema[29,30] and lymphedema.[31] Strain sensors provide additional information in such contexts. The following content provides systematic investigations of essential aspects of such classes of epidermal wireless passive sensors, including dielectric assessment of skin properties, hydration measurement, and skin strain induced by lymphedema due to subcutaneous fluid accumulation. Similar techniques, when combined with other sensing mechanisms, such as responses of ligand/receptor binding pairs,[32] dielectric changes in humidity or pH sensitive polymers,[33,34] and alignment changes within liquid crystals[35] can yield highly specific, stable, and repeatable, multimodal detection. External sensor readout systems can be adapted to wearable or portable configurations,[36,37] enabling compact and fully functional systems for health and wellness monitoring.

2. Design and Fabrication

The dielectric and strain sensors both exploit capacitive detection. The method used for dielectric determination is similar to that for measurement of input reflection through an open-ended coaxial line.[38] Here, the time varying electromagnetic fields created by a pair of planar electrodes generate periodic changes in current flow within the skin. The absorption of this energy by the skin depends on its dielectric properties. Sensing of strain relies on changes in the geometries of interdigitated electrode structures induced by deformations of the skin.[39] In both cases, the properties of the skin influence the capacitance of the sensing components, thereby leading to shifts in the resonance frequencies of the epidermal sensor.

2.1. Dielectric Measurement and Strain Determination

Figure 1 shows images and schematic illustrations of a multimodal wireless epidermal device that is 11.4 mm × 24.2 mm in overall dimension and consists of a dielectric sensor and a pair of strain sensors oriented perpendicular to each other. All three sensors are designed with distinct resonance frequencies, to enable separate readout without crosstalk. The dielectric sensor contains a pair of electrodes in the form of an inner circular disk (500 μm in radius) and an outer circular annulus (800 μm in inner radius and 1.2 mm in outer radius), both in direct contact

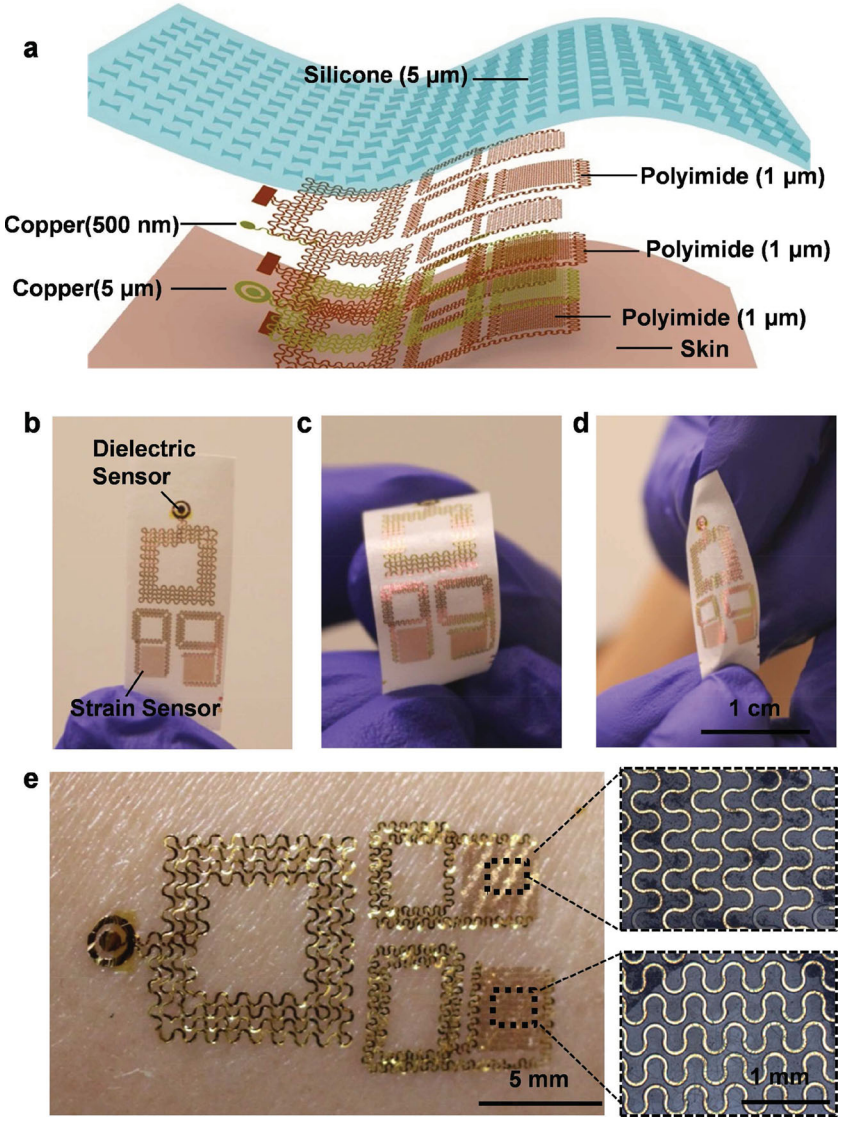

Figure 1. A multimodal wireless epidermal sensor. a) Exploded view schematic diagram of the sensor on the skin. Images of a sensor on a water soluble tape in b) flat, c) bent, and d) twisted configurations. e) Image of a sensor integrated directly on the skin, after removal of the tape.

with the skin, and connected to a coil encapsulated above and below by thin layers of polyimide. The coil consists of 4 turns of copper wire in a serpentine shape, to afford both flexibility and stretchability. The width of the wire is 150 μm, and the lengths of the inner and outer turns are 4.8 and 9.5 mm, respectively. The two strain sensors use serpentine interdigitated electrodes as deformable capacitors, oriented perpendicular to each other to allow sensing of strain in orthogonal directions. The coils for the strain sensors have 2 turns and 1.75 turns, respectively. The interdigitated electrodes formed by serpentine wire (40 μm in width) are approximately 3.2 mm in length with 13 digits and a uniform spacing of 300 μm between adjacent wires. The strain sensors are entirely encapsulated by polymer to prevent direct skin contact and, thereby, to reduce the influence of the skin dielectric properties on their response. The three sensors are separated to minimize the influence from mutual inductances generated by the nearby or enclosed coils, thereby improving the accuracy of wireless measurement

The fabrication starts with spin-coating a layer of polydimethylsiloxane (PDMS, 20 μm thick) onto a glass slide. Curing the PDMS and treating its surface with reactive ion etching (RIE) enables spin casting of a layer of polyimide (PI; 1 μm thick) on top (Figure S1a, Supporting Information). Serpentine interdigitated electrodes and circular electrodes consist of photolithographically patterned layers of copper (500 nm) deposited by electron beam evaporation (Figure S1b, Supporting Information). An additional coating of PI (1 μm) electrically insulates the surfaces of the electrode patterns; RIE removes selected regions of the PI to define points of electrical contact with the following metallization layer. Another patterned layer of copper (5 μm) forms serpentine coils (Figure S1c, Supporting Information), which are encapsulated by another PI coating. Etching of the entire system into an open mesh layout completes the main part of the fabrication (Figure S1d, Supporting Information). A water-soluble tape of cellulose (Aquasol ASWT-2) allows retrieval of the sensor from the PDMS substrate (Figure S1e, Supporting Information). Deposition of Ti/SiO_2 (5/60 nm) onto the exposed backside of the sensor by electron beam evaporation facilitates chemical bonding to an ultrathin perforated silicone substrate (5 μm in thickness) (Solaris, Smooth-On, Inc.) after UV ozone activation. Dissolving the cellulose tape with water yields an integrated device with excellent levels of mechanical stretchability and flexibility, to facilitate intimate contact with the skin (Figure S1f, Supporting Informartion).

2.2. Conformal Contact of the Wireless Epidermal Sensor to the Skin

The sensors can be integrated onto the skin with (**Figure 2**c) and without (Figures 1e, 2a) the backing layer of silicone. In many practical applications, the silicone provides protection against abrasion, in a way that imposes minimal constraint on transepidermal water loss or on natural motions of the skin. The mounting process involves placing the device into contact with the skin and then rinsing away the cellulose tape. Figure 2

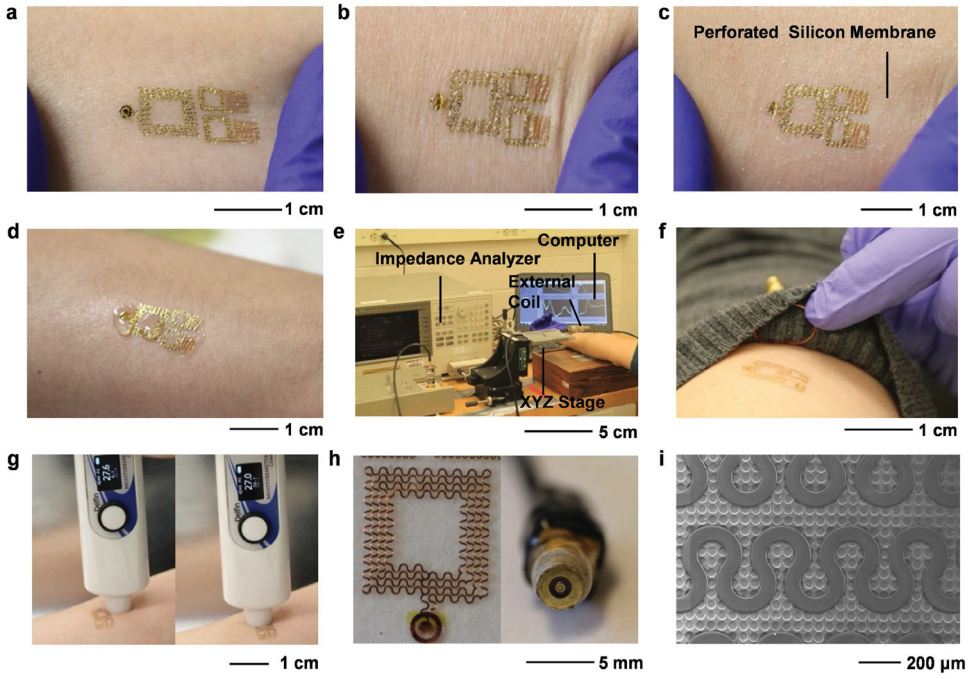

Figure 2. Images of a wireless epidermal sensor without a silicone backing layer on the skin in a a) stretched and b) squeezed state. c) Image of a device with a perforated silicone backing layer on the skin. d) Image of direct application of lotion onto a region of the skin that supports a device without a silicone backing layer. e) Experimental setup used for wireless measurement of the resonance frequency of the sensors. f) Picture of a copper coil sewn into clothing and connected with an impedance analyzer through a SMA connector, as an interface to a sensor mounted on the skin. g) A commercial hydration meter can be used to measure hydration at locations adjacent to or coincident with the position of a wireless epidermal sensor. h) Images of an epidermal dielectric sensor and an end-terminated coaxial cable with electrodes of similar dimension. i) Scanning electron micrograph of part of a wireless sensor on a perforated silicone backing layer.

shows the contact that results for cases with (Figure 2c) and without (Figure 2a) the silicone backing layer. In both cases, the device exhibits excellent contact and an ability to accommodate skin motion without delamination (Figure 2a–c). Absence of the silicone facilitates the diffusion of skin lotion and other media applied to the skin in the region of the device (Figure 2d), with nearly completely unimpeded transdermal water evaporation, in geometries that minimize thickness and effective modulus. Such a device configuration also enables direct reference measurements and comparison to skin evaluation using a commercial hydration meter (Delfin Moisture Meter SC), which is based on similar dielectric measurement principles but performed with a pair of rigid, circular electrodes applied to the same area of the skin (Figure 2g). Experiments described in the following exploit this capability.

2.3. Experimental Setup for Wireless Detection

The sensors are evaluated using an impedance analyzer (HP 4291a RF Impedance/Material Analyzer) with a frequency range from 1 MHz to 1.8 GHz. The analyzer connects to a hand-wound copper primary coil whose resonance frequency is significantly different from the epidermal wireless sensor. The impedance analyzer sweeps across 801 frequencies distributed linearly in the designated measurement frequency range. The signal amplitude (≈1 V) is sufficiently small to avoid any significant heating on the skin, as verified by thermal images (Figure S2a, Supporting Information) collected with an infrared camera (FLIR SC600). A xyz mechanical stage and a rotational platform allow manual adjustments of the position and orientation of the primary coil relative to the epidermal sensors (Figure 2e). The primary coil can be either positioned on this stage, for systematic studies, or it can be an accessory to clothing (Figure 2f), for more practical applications. The primary coil provides time varying electromagnetic fields that induce alternating voltages in the epidermal coils. Changes of the dielectric properties of the skin and/or mechanical strains lead to changes in the capacitances of the different sensing components and, therefore, their resonance frequencies. The operation should be carried out in ranges of frequencies where the dielectric properties are relatively frequency independent. In such ranges, the permittivity of the skin is determined primarily by water/fat content, hydration levels and other properties of interest.[40,41] A conventional sensor (Figure 2h) based on an open-ended coaxial cable equipped with a pair of electrodes with sizes matched to those of the epidermal dielectric sensor enables acquisition of comparative data.

The resonance frequency of the epidermal sensor is determined by the min-phase method,[42,43] in which a frequency (f_{min}) where the phase of the impedance of the primary coil reaches its minimum serves as an approximate measure of the resonance frequency of the epidermal sensor (f_0), given by

$$f_0 = 1/(2\pi\sqrt{L_E C_E}) \tag{1}$$

where L_E and C_E are the inductance and capacitance of the epidermal sensor, respectively. The impedance of the primary coil (Z_P) measured by the impedance analyzer can be expressed as

$$Z_P(\omega) = R_P + j\omega L_P + \omega^2 M^2/Z_E(\omega) \tag{2}$$

The impedance of the epidermal sensor (Z_E), the resistance (R_P), and inductance (L_P) of the primary coil all influence Z_P. The impedance of the epidermal sensor can be further expressed as:

$$Z_E(\omega) = R_E + j\omega L_E - j1/(\omega C_E) \tag{3}$$

The coupling coefficient (k) and the quality factor (Q) of the epidermal sensor can be expressed as

$$k = M/\sqrt{L_P L_E}$$
$$Q = \sqrt{L_E}/(R_E\sqrt{C_E}) \tag{4}$$

where M is the mutual inductance of the primary and epidermal coils. Terms in Equation 3 can then be written

$$L_E C_E = 1/\omega_0^2$$
$$R_E = \omega_0 L_E/Q \tag{5}$$

The impedance of the primary coil is

$$Z_P(\omega) = R_P + j\omega L_P\left[1 + k^2\omega^2/\omega_0^2(1 - \omega^2/\omega_0^2 + j\omega/\omega_0 Q)\right] \tag{6}$$

With a phase of $\angle Z_P$ be expressed as

$$\angle Z_P(\omega) = \arctan(\mathrm{Im}(Z_P(\omega)/\mathrm{Re}(Z_P(\omega)) \tag{7}$$

Setting the derivative of $\angle Z_E(\omega)$ to zero yields an expression for f_{min}. A Taylor series expansion provides a simple approximate relationship between f_{min} and f_0

$$f_{min} = f_0(1 + k^2/4 + 1/8Q^2) \tag{8}$$

Because the Q of the epidermal sensor is typically >20, the term $1/8Q^2$ can be neglected. The coupling coefficient k represents the efficiency of the interaction between two coils, and is thus $0 < k < 1$.[44] As a result, we can assume that $f_{min} \approx f_0$ for the rest of the analysis.[44] Variations in the phase of the impedance of the primary coil itself can be subtracted from the measured data by using a reference curve obtained from the primary coil evaluated without the presence of the epidermal sensors, in the same measurement location. This process eliminates the large background signal associated with the primary coil, thereby highlighting changes in phase caused by the epidermal sensor. In the following, shifts in phase relative to the reference phase of the primary coil are used, rather than the direct phase curve from the primary coil.

3. Results and Discussion

3.1. Measurements on the Body with Wired and Wireless Sensors

As a first example, the wireless sensor is used to define the dielectric properties of the skin at various positions across the

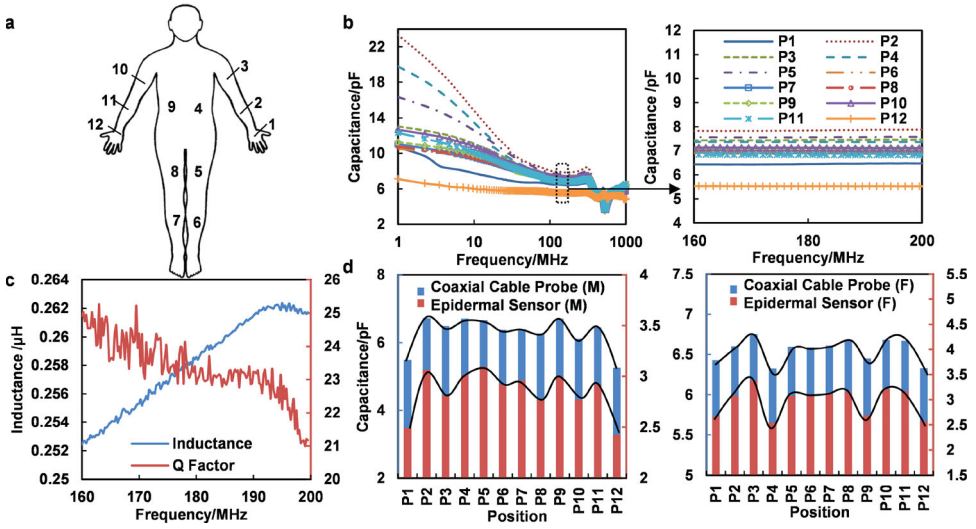

Figure 3. a) Diagram of 12 different positions for measurements of the skin. b) Representative variations in dielectric properties of the skin for frequencies between 1 MHz to 1 GHz, evaluated using a coaxial cable probe, at the positions illustrated in (a). Minimal variations occur between 160 MHz to 200 MHz, as shown on the right. c) Plot of the inductance and Q factor of the epidermal dielectric sensor between 160 MHz to 200 MHz. d) Comparison of capacitance measured using a wireless sensor and a coaxial cable for two volunteers (M for male; F for Female), at the positions indicated in (a).

body for two male and two female volunteers, at 12 regions (**Figure 3**a). The coaxial sensor (Figure 2h) provides comparison data. For measurement frequencies between 1 MHz and 1 GHz, the dielectric properties of the skin show clear variations with frequencies and positions, for all four volunteers. A typical spectrum, as in Figure 3b, measured with the coaxial cable exhibits a rapidly decreasing dielectric constant at low frequencies (from 1 to 90 MHz), followed by more modest frequency dependence at higher frequencies. The smallest dependence occurs in a range of frequencies between 160 to 200 MHz, where the capacitance varies by only ≈0.6% (Figure 3b). The observed stability of the skin dielectric properties between 160 to 200 MHz may be due to the dominant effect of δ dispersion of bonded and free dipolar water molecules,[45,46] while other frequency-dependent polarization effects are not significant. These trends are similar to those reported elsewhere.[41,46] The epidermal dielectric sensor is designed with a resonance frequency that lies within this region of minimal frequency dependence.

Measurements collected with the wireless sensor exhibit changes in resonance frequency with position across the body, due to variations in water and fat contents of the skin (Figure 3a). The capacitance of the sensor can be obtained from Equation 1 using its resonance frequency and separate measurements of the inductance of the sensor. This inductance, which is determined using the impedance analyzer (Figure 2c), is assumed to be less sensitive[13] to changes of skin dielectric properties due to its lack of direct contact with the skin. Electrical simulation using HFSS (Ansys Inc.) further confirms that the S11 parameter, which is directly related to the impedance of the coil, undergoes little change when the skin changes from a dry to a wet state (Figure S3, Supporting Information). The capacitance determined in this way can be compared to that measured using the coaxial cable probe, at the same frequencies. Trends of capacitance variation with position (Figure 3d) as measured by the coaxial cable and the epidermal sensor are consistent, as expected. However, symmetry in measurement locations does not lead to symmetrical responses due to strong location dependent properties of skin tissues.

3.2. Measurements of Skin Hydration

To demonstrate an important mode of measurement, the wireless sensor is used to evaluate the level of hydration of the skin at a position 2 (Figure 3a) on the forearm. Application of lotion induces variations in hydration levels, which can then be evaluated as a mean to illustrate the measurement capability.[10,47] The hydration levels are recorded using both a wireless epidermal sensor and a commercial hydration meter. As the hydration level changes from 103 to 31 (arbitrary unit given by the hydration meter), f_0 of the device shifts from 163 to 176 MHz (**Figure 4**a,b), indicating a decrease in the capacitance and, therefore, the skin dielectric constant, consistent with a decrease in the water content (i.e., hydration). f_0 shows little variation, even in the relatively uncontrolled environment of the lab, where mechanical vibrations and temperature fluctuations are present (Figure S6a, Supporting Information). f_0 of the dielectric sensor changes only by approximately 1 MHz for a temperature change of 10 °C (Figure S2b, Supporting Information). The measured f_0 can be determined easily with a precision of 0.2 MHz, which corresponds to a precision in hydration measurement that is equivalent to 1.1 (arbitrary unit) on the scale of the commercial hydration meter. The hydration measurement result is conducted under lab environment where the humidity is relatively stable. To investigate the effects of humidity, the surface of a device exposed to air was passivated by polyimide and covered with a perforated silicone layer. This construction prevents direct contact between the electrodes and the air, and thus reduces the response of the sensor to the humidity. Assessment with humidity levels between 22% to 88% indicated a change in f_0 of ≈5.8 MHz (Figure S4,

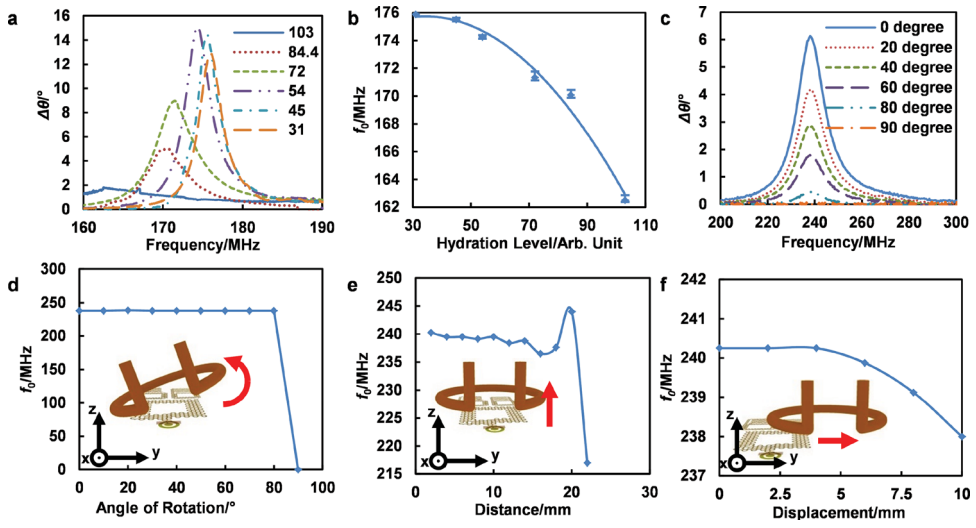

Figure 4. a) Measurements of the phase response of the primary coil, while in proximity to an epidermal dielectric sensor on the skin, at different levels of hydration. The magnitude of the phase difference changes both with dielectric properties of the skin and the distance between the primary coil to the epidermal sensor. As a result, variations in the magnitude can arise from inconsistencies in the placement of the measured forearm. b) Relationship between the minimum phase f_0 and hydration levels measured using a commercial hydration sensor. c) Phase response of the primary coil oriented at different angles relative to the epidermal dielectric sensor. Measured shifts in f_0 as the primary coil is displaced d) rotationally, e) vertically, and f) horizontally. The assessment of the influence of sensor orientation is conducted on a stretching stage in air. The resonance frequency of the sensor is relatively high(at approximately 240 MHz) when measured in air. The resonance frequency is between 160–200 MHz when placed on skin.

Supporting Information). Such changes can be compensated using separate measurements of the humidity. We note that the air humidity will also influence the hydration of the skin.

3.3. In-Vitro Characterization of the Sensor Responses

According to Equation 8, the measurement depends critically on the coupling coefficient between the epidermal sensor and the primary coil. The relative position between the coils is, therefore, important. In-vitro characterization of the effects is possible through measurements conducted with the wireless sensor on a flat glass substrate, while systematically varying the position of the primary coil. To examine the influence of rotation, the sensor is placed underneath the primary coil at a fixed distance of 8 mm. The rotation of the primary coil is then adjusted using a precision stage. Figure 4c shows that the quality factor of the phase curve decreases with counter clockwise rotation around an axis that passes through the center of the primary coil and aligns parallel with the x direction. The measured f_0 remains at 238 MHz for rotations between 0 to 80°, but then changes rapidly for larger angles (Figure 4d). Uniaxial displacements along the z (vertical displacement) (Figure 4e) and y (horizontal displacement) (Figure 4f) directions of the primary coil, originally placed 2 mm above the epidermal sensor, are achieved with the xyz mechanical stage. Little change in f_0 is observed for a horizontal displacement of up to 1.4 cm and a vertical displacement of up to 0.4 cm, followed with a significant decrease in f_0 and Q factor beyond these limits (Figure S5a,b, Supporting Information). This measurement demonstrates a robust range of displacements and angles over which reliable wireless detection can be achieved, with changes of f_0 less than 0.4%.

The capability of the strain sensors in detecting directional strains in the skin are evaluated with a mechanical stage (**Figure 5**a) to create well defined levels of uniaxial strain in the devices. Here, fixtures constrain the sensor at both ends, in a suspended configuration. The dielectric and strain sensors all stretch by ≈30% of their original length; the end-to-end displacement of the overall system is ≈48%. The dielectric sensor exhibits only a 0.2% variation in its f_0 (230 MHz) under stretching in both x and y directions for strains up to 30% (**Figure 6**a). The limited influence of the strain in this case may be due to the symmetric layout of the sensor (Figures S8,S9, Supporting Information). The results suggest an ability of the sensor to provide dielectric measurements with high tolerance to strain.

By contrast, the strain sensors (denoted as sensor 1 and sensor 2 in Figure 5a) exhibit high sensitivity to stretching. For example, stretching sensor 1 by 29.1% along the x direction (Figure 5c,d) leads to a decrease in f_0 by 22.7 MHz (4.2% of f_0 at static state). Here, the spacings between the electrodes of sensor 2 also have a maximum change of 29.1% (16% in certain region as shown in Figure 5b,e), thereby leading to an increase in its resonance frequency of 22.5 MHz (3.4% of f_0 at static state) (Figure 5c,d). The sensors respond in a corresponding manner for extension along the y direction. Consideration of the nature of the mechanical deformations of the individual electrodes provides an explanation for these observations. Electrodes that lie along the direction of stretching experience an increase in their end-to-end length as well as reduction in their spacing, as shown in Figure 5e. These deformations result in an increase in capacitance and decrease in f_0. Reversed changes for electrodes aligned perpendicular to the stretching direction are observed due to the Poisson's effect. This deformation causes an increase in electrode spacings and reduction in their overall lengths, thereby leading to a decrease in sensor

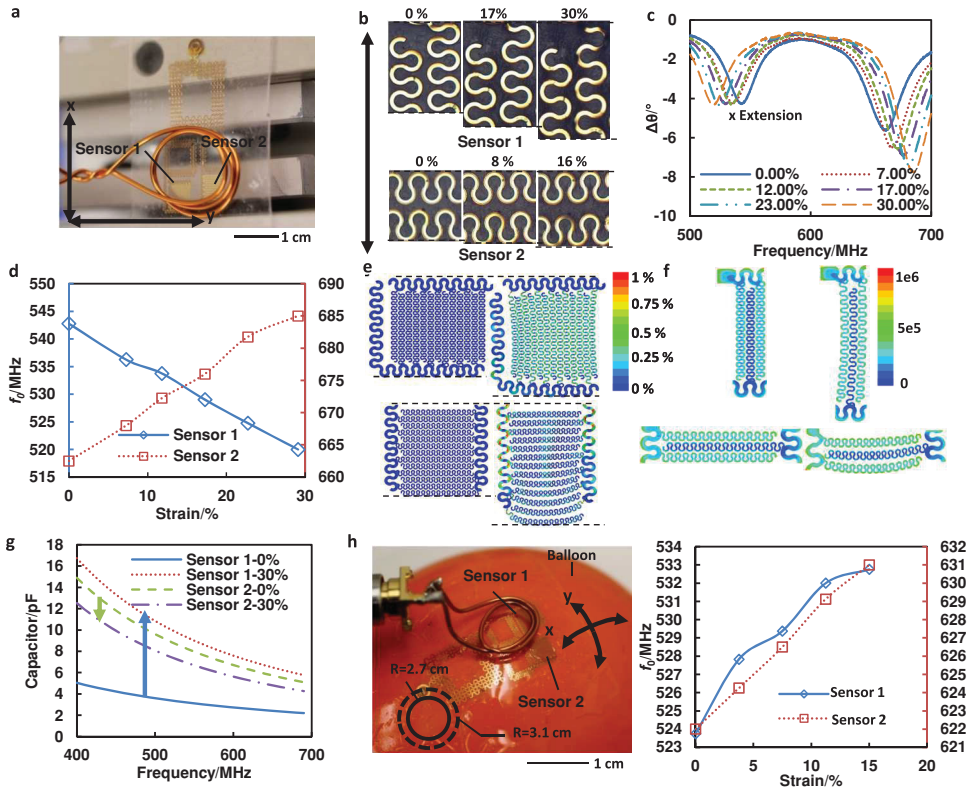

Figure 5. a) Experimental setup to characterize the response of the strain sensors as a function of extension along the *x* and *y* directions. b) Images of the strain sensors under 0 to 30% uniaxial stretch along the *x* direction. c) Frequency response and d) resonance frequency shift of the strain sensors for extensions between 0 to 30% along the *x* direction. e) Finite element simulation of strains for extensions between 0 to 30% along the *x* direction. f) Finite element simulation of the redistribution of the electrical field in structures similar to those for the strain sensors for extensions between 0 to 30% along the *x* direction. g) Simulated changes in capacitance associated with these structures. h) Image of a wireless epidermal sensor attached onto the surface of a balloon to simulate measurement of lymphedema (left), and change in resonance frequencies of strain sensors under the expansion of the balloon (right).

capacitance and an increase in the f_0. Simulations can capture these behaviors. To simplify the calculations, segments of structures extracted from the finite element simulation (FEM) results of Figure 5e are used for electrical simulation with HFSS (Ansys Inc.) to determine the associated electrical field distributions (Figure 5f) and capacitance changes (Figure 5g). Results from Figure 5g indicate that electrodes aligned with the extension direction undergo larger capacitance changes than electrodes oriented perpendicular to the extension, suggesting that the combined effect of the electrode length increase and the spacing reduction may be more prominent in changing the sensor capacitance than the effects of reduced electrode length and increased spacing.

The strain sensors exhibit low drift over measurement periods of several hours, with random fluctuations in f_0 of approximately 1 MHz (Figure S6b,c, Supporting Information), suggesting a strain measurement precision of 1.3%. Systematic drifts are not observed. The fluctuations in the responses of the strain sensors are larger than those in the dielectric sensor (0.2 MHz). This observation suggests that the complex interdigitated structures in the strain sensors may be less tolerant to enviromental disturbances than the symmetrical configuration of the dielectric sensor.

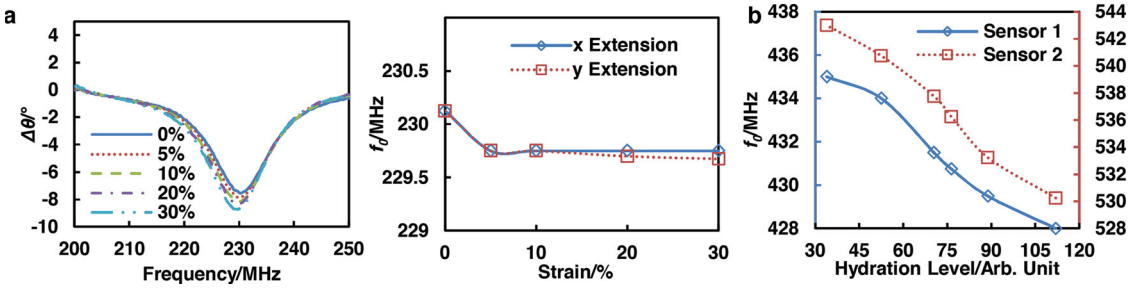

Figure 6. a) Phase response of the primary coil when the dielectric sensor is under various levels of uniaxial tension (left), and the shift of the resonance frequency as a function of strain (right). b) Dependence of the resonance frequencies of a strain sensor on hydration of the skin.

The influence of changes in dielectric properties on the response of the strain sensors appear in Figure 6b at escalated skin hydration levels. The results reveal monotonic decreases in f_0 of both sensors as a result of the increase in the capacitance of the sensors. The influence of skin hydration on the strain sensors can be compensated by adding or subtracting bias values that correspond to the strain-independent skin hydration results measured by the dielectric sensor (Figures 4a, 6a). In addition, increasing the thickness of the passivation layer of the strain sensor can further reduce the hydration-induced changes in strain sensors. FEM simulation results of stretching the end-to-end length of the device by 30% in a uniaxial manner (Figures S8,S9, Supporting Information) indicate that the average principal strain in the metals is less than the fracture strain of Cu (≈2%), suggesting an ability to offer robust operation at strain levels well beyond those that can be tolerated by the skin (10–20%). The strain reaches 3.3% and 1.7% in certain localized regions, due to stress/strain concentrations at the edges or corners, but with limited observed ability to cause facture. In addition, the symmetric structures of the coils of all sensors under uniaxial extension suggest that the changes in the coil properties in one direction may be compensated by the coil property changes in perpendicular direction. This behavior may explain the strain-independent results of the dielectric sensor as observed in Figure 6a. Electrical simulation of the entire sensor structures under different strain using HFSS can provide important information related to strain induced electrical property change. However, this computation involves considerably larger numbers of vectors and additional computation resources. Such studies represent topics of on-going work.

3.4. Strain Sensing with Simulated Lymphedema

Lymphedema, a common condition for patients after axillary surgery and radiation therapy, is due to chronic retention and swelling of localized lymphatic system fluids. The symptomatic gradual swelling of arms and legs is not immediately observable, and continuous monitoring is currently not possible. The wireless epidermal strain sensors provide an effective solution. A balloon filled with water approximates conditions associated lymphedema-swelling of the skin.[48] Here, the strain sensors lie at the position of the maximum perimeter of the balloon (γ direction in Figure 5h). Increasing the maximum balloon radius (γ direction) from 2.7 cm to 3.1 cm by injecting 40 mL water induces changes in the resonance frequencies of the sensors from 524 and 632 MHz to 532 and 637 MHz, respectively. Approximating the balloon as a sphere with uniform expansion suggests that a 15% increase in the radius of the balloon leads to 15% stretching along both x and y directions. These results indicate that the strain sensors have the potential to quantify multi-axial strains caused by tissue swelling due to accumulation of water. The changes in the responses of the strain sensors with expansion of balloon involve multi-axial stress and three-dimensional deformation. Thus, the direction and value of the principle strain cannot be determined using the current device configuration. Further understanding of the behaviors of the strain sensors on inflatable objects can lead to applications that involve tissue swelling and implantable stents, and represent important aspect of current work.

4. Conclusion

The wireless passive sensor technology introduced here provides a soft, "skin-like" device that enables intimate integration with the skin and non-invasive, wireless quantification of skin dielectric properties related to water contents and mechanical strains induced by excessive subcutaneous fluid accumulation (lymphedema). The sensors exhibit some tolerance to misalignment with the primary coil, as required for practical use in wearable applications. With a maximum voltage level of 1 V output from the impedance analyzer, the measurement distance between the primary coil and the epidermal sensor is limited to 1.4 cm. One attractive possibility for use outside of a laboratory setup might involve near field communication (NFC) techniques that are available in many portable consumer electronic devices. In addition, when combined with other biomolecule recognition and chemical sensing techniques, this type of epidermal wireless sensor can be constructed as a multifunctional sensing patch, with potentially important uses in continuous health monitoring.

Supporting Information

Supporting Information is available from the Wiley Online Library or from the author.

Acknowledgements

The authors would like to acknolwedge the support from the MC10, Inc. and the Gates Foundation. Y.G.H. thanks the support from NSF (DMR-1242240). H.Y.C. is supported by a international student fellowship from Howard Hughes Medical Institute. This work was conducted in part in the Frederick Seitz Materials Research Laboratory Central Facilities, University of Illinois.

Received: November 17, 2013
Revised: January 14, 2014
Published online: March 2, 2014

[1] D. Khodagholy, T. Doublet, P. Quilichini, M. Gurfinkel, P. Leleux, A. Ghestem, E. Ismailova, T. Herve, S. Sanaur, C. Bernard, G. G. Malliaras, *Nat. Commun.* **2013**, *4*, 1575.
[2] D. Khodagholy, T. Doublet, M. Gurfinkel, P. Quilichini, E. Ismailova, P. Leleux, T. Herve, S. Sanaur, C. Bernard, G. G. Malliaras, *Adv. Mater.* **2011***23*, H268.
[3] G. Liang, G. S. Guvanasen, L. Xi, C. Tuthill, T. R. Nichols, S. P. DeWeerth, *IEEE Trans. Biomed. Circuits Syst.* **2013**, *7*, 1.
[4] G. S. Jeong, D. H. Baek, H. C. Jung, J. H. Song, J. H. Moon, S. W. Hong, I. Y. Kim, S. H. Lee, *Nat. Commun.* **2012**, *3*, 977.
[5] H. C. Jung, J. H. Moon, D. H. Baek, J. H. Lee, Y. Y. Choi, J. S. Hong, S. H. Lee, *IEEE Trans Biomed Eng* **2012**, *59*, 1472.
[6] J.-H. Moon, D. H. Baek, Y. Y. Choi, K. H. Lee, H. C. Kim, S.-H. Lee, *J. Micromech. Microeng.* **2010**, *20*, 025032.
[7] R. C. Webb, A. P. Bonifas, A. Behnaz, Y. Zhang, K. J. Yu, H. Cheng, M. Shi, Z. Bian, Z. Liu, Y. S. Kim, W. H. Yeo, J. S. Park, J. Song, Y. Li, Y. Huang, A. M. Gorbach, J. A. Rogers, *Nat. Mater.* **2013***12*, 938.

[8] D. H. Kim, N. Lu, R. Ma, Y. S. Kim, R. H. Kim, S. Wang, J. Wu, S. M. Won, H. Tao, A. Islam, K. J. Yu, T. I. Kim, R. Chowdhury, M. Ying, L. Xu, M. Li, H. J. Chung, H. Keum, M. McCormick, P. Liu, Y. W. Zhang, F. G. Omenetto, Y. Huang, T. Coleman, J. A. Rogers, *Science* **2011**, *333*, 838.
[9] T. F. Tadros, in Colloids in Cosmetics and Personal Care, Wiley-VCH Verlag GmbH & Co. KGaA, Weinheim **2008**.
[10] X. Huang, H. Cheng, K. Chen, Y. Zhang, Y. Liu, C. Zhu, S. c. Ouyang, G. W. Kong, C. Yu, Y. Huang, J. A. Rogers, *Biomed. Eng., IEEE Trans.60*, 2848.
[11] D. H. Kim, N. Lu, R. Ma, Y. S. Kim, R. H. Kim, S. Wang, J. Wu, S. M. Won, H. Tao, A. Islam, K. J. Yu, T. I. Kim, R. Chowdhury, M. Ying, L. Xu, M. Li, H. J. Chung, H. Keum, M. McCormick, P. Liu, Y. W. Zhang, F. G. Omenetto, Y. Huang, T. Coleman, J. A. Rogers, *Science* **2011** *333*, 838.
[12] W.-H. Yeo, Y.-S. Kim, J. Lee, A. Ameen, L. Shi, M. Li, S. Wang, R. Ma, S. H. Jin, Z. Kang, Y. Huang, J. A. Rogers, *Adv. Mater.* **2013**, *25*, 2773.
[13] E. Tan, W. Ng, R. Shao, B. Pereles, K. Ong, *Sensors* **2007**, *7*, 1747.
[14] C. Po-Jui, S. Saati, R. Varma, M. S. Humayun, T. Yu-Chong, *J. Microelectromech. Syst.* **2008**, *19*, 721.
[15] C. Po-Jui, D. C. Rodger, S. Saati, M. S. Humayun, T. Yu-Chong, *J. Microelectromech. Syst.* **2008**, *17*, 1342.
[16] K. G. Ong, K. Zeng, C. A. Grimes, *IEEE Sensors J.* **2002**, *2*, 82.
[17] S.-H. Song, G. T. Gillies, M. R. Begley, M. Utz, W. C. Broaddus, *J. Med. Eng. Technol.* **2012**, *36*, 156.
[18] K.-H. Shin, C.-R. Moon, T.-H. Lee, C.-H. Lim, Y.-J. Kim, *Sens. Actuators A Phys.* **2005**, *123–124*, 30.
[19] N. Najafi, A. Ludomirsky, *Biomed. Microdevices* **2004**, *6*, 61.
[20] R. P. Patterson, *IEEE Eng. Med. Biol. Mag.* **1989**, *8*, 35.
[21] D. T. Nguyen, C. Jin, A. Thiagalingam, A. L. McEwan, *Physiol. Meas.* **2012**, *33*, 695.
[22] D. D. Pak, N. I. Rozhkova, M. N. Kireeva, M. V. Ermoshchenkova, A. A. Nazarov, D. K. Fomin, N. A. Rubtsova, *Biomed. Eng.* **2012**, *46*, 154.
[23] Ø. G. Martinsen, S. Grimnes, E. Haug, *Skin Res. Technol.* **1999**, *5*, 179.
[24] D. Miklavčič, N. Pavšelj, F. X. Hart, in Wiley Encyclopedia of Biomedical Engineering John Wiley & Sons, Inc. Hoboken, NJ **2006**.
[25] M. Guihan, B. M. Bates-Jenson, S. Chun, R. Parachuri, A. S. Chin, H. McCreath, *J. Spinal Cord Med.* **2012**, *35*, 46.
[26] A. Papp, T. Lahtinen, M. Harma, J. Nuutinen, A. Uusaro, E. Alhava, *Plast Reconstr. Surg.* **2006**, *117*, 889.
[27] A. P. Colbert, J. Yun, A. Larsen, T. Edinger, W. L. Gregory, T. Thong, *Evid. Based Complement Alternat. Med.* **2008**, *5*, 443.
[28] S. Pearson, A. P. Colbert, J. McNames, M. Baumgartner, R. Hammerschlag, *J. Altern. Complement Med.* **2007**, *13*, 409.
[29] H. N. Mayrovitz, S. Davey, E. Shapiro, *Clin. Physiol. Funct. Imaging* **2008**, *28*, 337.
[30] H. N. Mayrovitz, M. Bernal, F. Brlit, R. Desfor, *Skin Res. Technol.* **2012**, *19*, 47.
[31] H. N. Mayrovitz, S. Davey, E. Shapiro, *Clin. Physiol. Funct. Imaging* **2009**, *29*, 123.
[32] X. Huang, S. Li, J. S. Schultz, Q. Wang, Q. Lin, *Appl. Phys. Lett.* **2010**, *96*, 033701.
[33] Z. Chen, C. Lu, *Sensor Lett.* **2005**, *3*, 274.
[34] S. Bhadra, G. E. Bridges, D. J. Thomson, M. S. Freund, *J. Nanotechnol. Eng. Med.* **2011**, *2*, 011011.
[35] A. S. Abu-Abed, R. G. Lindquist, *IEEE Sensors J.* **2008**, *8*, 1557.
[36] E. Sardini, M. Serpelloni, *IEEE Trans. Instrum. Meas.* **2012**, *61*, 2354.
[37] R. Nopper, R. Has, L. Reindl, *IEEE Trans. Instrum. Meas.* **2011**, *60*, 2976.
[38] M. A. Stuchly, T. W. Athey, S. S. Stuchly, G. M. Samaras, G. Taylor, *Bioelectromagnetics* **1981**, *2*, 93.
[39] L. L. Chu, Q. Long, Y. B. Gianchandani, *J. Microelectromech. Syst.* **2002**, *11*, 489.
[40] S. Takahiro, I. Hiroo, F. Shigeo, S. Hiroshi, K. Hirotada, M. Yoshinaga, Y. Eiji, O. Takayuki, T. Shuji, M. Hajime, S. Yasuhito, *Phys. Med. Biol.* **2002**, *47*, N11.
[41] C. Gabriel, S. Gabriel, E. Corthout, *Phys. Med. Biol.* **1996**, *41*, 2231.
[42] T. J. Harpster, B. Stark, K. Najafi, *Sens. Actuators A Phys.* **2002**, *95*, 100.
[43] E. Sardini, M. Serpelloni, *Sensors* **2009**, *9*, 943.
[44] R. Nopper, R. Niekrawietz, L. Reindl, *IEEE Trans. Instrum. Meas.* **2010**, *59*, 2450.
[45] C. Cametti, S. Marchetti, C. M. C. Gambi, G. Onori, *J. Phys. Chem. B* **2011**, *115*, 7144.
[46] E. H. Grant, *Bioelectromagnetics* **1982**, *3*, 17.
[47] X. Huang, W.-H. Yeo, Y. Liu, J. Rogers, *Biointerphases* **2012**, *7*, 1.
[48] A. G. Warren, H. Brorson, L. J. Borud, S. A. Slavin, *Ann. Plast. Surg.* **2007**, *59*, 464.